Impact of Estuarine Dams on the Estuarine Parameter Space and Sediment Flux Decomposition: Idealized Numerical Modeling Study

Steven M. Figueroa[1], Guan-hong Lee[1*], Jongwi Chang[1], Kenneth D. Lagamayo[1], Nathalie W. Jung[1]

[1]Department of Oceanography, Inha University, Incheon, South Korea

[*]Corresponding author: G. Lee (ghlee@inha.ac.kr)

Key Points:

- Estuarine dams reduce tidal currents and cause unsteady freshwater discharge
- Post-dam estuaries tend to be salt wedge estuaries during discharge and bays during no discharge
- Estuarine dams reduce exchange flow and Stokes transport sediment fluxes and increase river runoff and tidal pumping sediment fluxes

1. Abstract

Estuarine dams can result in profound changes to estuarine environments. However, their impact on estuarine currents, stratification, and sediment fluxes is not well understood. To develop a general understanding, an idealized modeling study was carried out using the Coupled-Ocean-Atmosphere-Wave-Sediment Transport Modeling System. Idealized estuarine geometry was based on 10 estuaries with estuarine dams. Tide and river forcing were varied to produce strongly stratified, partially mixed, periodically stratified, and well-mixed estuaries. Each model ran for one year. Next, the models were subject to the construction of an estuarine dam and run for another year. Then, the pre- and post-dam conditions were compared. Results showed that estuarine dams amplify the tidal range and reduce the tidal currents. The post-dam estuaries tended to be salt wedge and strongly stratified types during freshwater discharge, but during no freshwater discharge they became fjord, bay, or periodically stratified types based on the estuarine parameter space. For all estuaries, the estuarine turbidity maximum moved seaward, and the suspended sediment concentrations tended to decrease. While the depth changes depended on the estuary type, the surficial sediment texture shifted to being muddier for all types. In terms of sediment flux mechanisms, the estuarine dam reduced the exchange flow and Stokes transport. The estuarine dam also increased the seaward river runoff for cases with strong river, and increased the landward tidal pumping for cases with strong tides. This study is one of the first to generalize the effect of estuarine dams to a range of estuarine types.

Plain-language summary

Estuaries are where rivers flow into the sea. Recently, humans have built dams on estuaries to block salt water from traveling upstream. This secures freshwater resources. However, it can cause significant changes to estuaries. To better understand how estuarine dams affect estuaries this study used a simplified computer model of an estuary. We changed the strength of their tides and river currents to look at different types of estuaries ranging from an estuary with a strong river to an estuary with strong tides. After putting an estuarine dam in the models, we compared the estuaries before and after the estuarine dam. It was found that estuarine dams made the tidal currents weaker in all the estuaries. They also changed the freshwater discharge from being steady to alternating between periods of high discharge and periods of no discharge. These changes overall resulted in the estuaries being stratified during discharge and being like a bay during no discharge. Also, the reduced tidal currents resulted in less sediment in the water column and the deposition of mud on the bed. These findings show that estuarine dams can cause significant changes to estuaries, which has important implications for estuarine fisheries and shipping.

Index Terms: 4235 Estuarine processes; 4255 Numerical modeling; 4323 Human impact; 4558 Sediment transport

Keywords: Idealized estuary, Estuarine dam, Estuarine parameter space, Sediment flux decomposition

1. Introduction

Estuaries are regions where rivers flow into the coastal ocean. The physical functioning of estuaries varies greatly and depends on the estuary size, shape, sedimentary characteristics, and external physical forcing by the river, tides, waves and wind (Wolanski & Elliot, 2016). The net result of these features gives the overall water circulation patterns. Sediments are important in estuaries because sediment flux gradients contribute to the depth and texture of the bed and the overall turbidity of the water column which in turn affects estuarine fisheries and navigability. At present, sediment fluxes are changing in estuaries, as humans have modified the shape of estuaries worldwide through activities such as land reclamation, dredging, and the construction of hard engineering structures (Jung et al., 2021; Wang et al., 2015). Land reclamation and dredging are often carried out to create space and improve navigability (Winterwerp & Wang, 2013), while hard engineering structures such as breakwaters, riprap, jetties, and seawalls have been designed to absorb wave energy and stabilize the coast (Davis Jr. & Fitzgerald, 2019). In addition to these modifications, several across-channel structures have been built in the channels near river mouths such as tidal power plants, storm surge barriers, and estuarine dams for purposes of electricity generation, flood protection, and blocking the salt intrusion to secure freshwater resources, respectively (Morris, 2013).

Estuarine dams are defined here as dams constructed within either the salt or tidal intrusion limits of an estuary. As salt and tidal intrusions in estuaries are commonly on the order of 1 - 100 km (Prandle, 2009), estuarine dams are

typically located within this distance from the coast. Estuarine dams were constructed primarily during the latter half of the 1900s, resulting in the shortening of estuaries. Estuarine dams are both numerous and globally distributed. For example, there are around 320 estuarine dams along the coast of China (Tilai et al., 2019; Zhu et al., 2017) and about half of the estuaries along the coast of South Korea are closed by estuarine dams (Lee et al., 2011). Estuarine dams can also be found at the mouths of well-known rivers including the Murray-Darling rivers (Webster, 2005), the Senegal River (Barusseau et al., 1998), and the Rhine Meuse rivers (Tönis et al., 2002).

Although constructed worldwide in the past century, only a handful of estuaries with an estuarine dam have been analyzed regarding the effects of the estuarine dam on the hydrodynamic and sedimentary environments. Available case studies indicate that estuarine dams can result in tidal amplification due to reflection of the tidal wave (Díez-Minguito et al., 2012; Kang, 1999; Kwon and Lee, 1999), reduction of tidal currents due to loss of the tidal prism, and change in the magnitude of tidal asymmetry due to altered tidal and river forcing (Kang, 1999; Kim et al., 2006; Traini et al., 2015). In turn, altered tidal and river forcing has been inferred to change the salinity structure and estuarine type (Shin et al., 2019), including the potential to develop periodic stratification (Figueroa et al., 2019, 2020a). Furthermore, the reduced tidal currents and estuarine dam discharge have been observed to result in lower suspended sediment concentration (SSC; Kim et al., 2006; Traini et al., 2015), increasing fluvial sediment abundance (Williams et al., 2014), and enhanced deposition of fine sediment in the remnant estuary (Kim et al., 2006; Lee and Lee, 2007; Tilai et al., 2019; van Proosdij et al., 2009; Williams et al., 2013, 2014; Zhu et al., 2017). Such deposition may depend on the tidal range and river discharge, as suggested by available sediment flux studies. For example, in a microtidal estuary with relatively large freshwater discharge, sediment flux convergence can occur due to a negative gradient in the seaward advective sediment flux driven by river runoff (Williams et al., 2015; Chang et al., 2020). In contrast, in a macrotidal estuary with moderate freshwater discharge, sediment flux convergence can occur due to a negative gradient in the landward tidal pumping sediment flux driven by tidal asymmetry (Figueroa et al., 2020a, 2020b; Zhu et al., 2017).

Limited field observations together with the diversity of estuary types and their complex physical processes has hampered a general understanding of the effect of estuarine dams on estuarine sedimentary environments. While field measurements are essential, numerical sediment transport models can complement field observations and have several advantages. First, they provide the opportunity to investigate the estuaries under different forcing conditions as well as before and after dam construction. Second, they provide greater data coverage for analysis compared to field measurements. And third, investigation of simplified, idealized estuaries can provide insight into the basic physical processes which can be obscured in complex, real estuaries (e.g., Burchard & Baumert, 1998; Chen & Sanford, 2009; Hetland & Geyer, 2004; Huijts et al., 2006; Tarpley et al., 2019).

Therefore, the objective of this study is to clarify the effect of estuarine dams on a range of estuarine types via simplified, idealized estuaries. To understand the effect of an estuarine dam on different estuarine types, scenarios with different tidal range and river discharge were implemented, and the results before and after the estuarine dam were compared. With the greater data availability provided by the idealized models, attention was given to changes in estuarine type and sediment flux mechanisms due to the estuarine dam which has previously not been analyzed for a range of estuarine types. For a range of estuarine types, the research questions of this study are: 1) how does an estuarine dam affect the tidal currents, stratification, and estuarine type?; 2) how does an estuarine dam affect the estuarine SSC, bed level, surficial grain size, and abundance of fluvial sediment?; and 3) how does an estuarine dam affect the estuarine sediment flux mechanisms?

This paper is organized as follows. Section 2.1 described the model, model settings, and model scenarios. Section 2.2 presents the method to quantify the impact of the estuarine dams on estuarine type and estuarine sediment flux mechanisms. Then, Section 3 compares the pre- and post-dam results. Section 4 discusses the significance and implications of this study and compares this study with other studies. Finally, Section 5 summarizes the main conclusions.

2. Materials and methods

2.1. Data collection

2.1.1. Model description

The Coupled-Ocean-Atmosphere-Wave-Sediment Transport (COAWST) modeling system is comprised of several components that include models for the ocean, atmosphere, surface waves, and sediment transport (Warner et al., 2010). This study utilized only the ocean and sediment transport models. The ocean model is the Regional Ocean Modeling System (ROMS). ROMS is a free surface, terrain-following numerical model that solves the three-dimensional Reynolds-averaged Navier-Stokes equations using the hydrostatic and Boussinesq approximations (Haidvogel et al., 2008). The sediment transport model is the Community Sediment Transport Modeling System (CSTMS), which computes suspended sediment transport using the advection-diffusion algorithm applied to all passive tracers together with an additional algorithm for vertical settling (Warner et al., 2008, 2010). The sediment transport algorithms are implemented for an unlimited number of user-defined sediment classes. CSTMS may be implemented with noncohesive, cohesive, and mixed sediments (Sherwood et al., 2018). However, at present, modeling mixed and cohesive sediment transport adds significant computational expense (Tarpley et al., 2019), therefore this study did not include these processes.

2.1.2. Model domain and setup

Figure 1 illustrates the model domain for both the pre- and post-dam conditions. The idealized estuary was funnel shaped with a curved ocean boundary. The

origin at $x = 0$ km was located at the widest point of the domain. The domain extended to $x =$ -15 km on the seaward side, and to $x = 250$ km on the landward side. The width of the estuary decreased exponentially from 30 km to 1 km wide from $x = 0$ km to $x = 30$ km. Beyond $x = 30$ km the width stayed uniform. From $x =$ -15 km to $x = 100$ km, the thalweg depth decreased linearly from 10 m to 5 m. Then, from $x = 100$ km to $x = 250$ km the thalweg depth was a constant 5 m. The across-channel shape was Gaussian such that there were 0.1 km wide intertidal areas at each bank.

To determine the position of the estuarine dam in the model, historical and geometric data for 10 real estuaries with estuarine dams was compiled (Figure 2, Table 1). It was found based on these estuaries that the pre- and post-dam estuarine lengths were nominally 100 km and 20 km, respectively. At the same time the mean estuarine mouth width was found to be 2 km. Therefore, the mouth of the estuary was located where the width was 2 km. The location of the estuarine dam was then defined to be 20 km upstream from the mouth and the nominal length of the pre-dam estuary was defined to be 100 km upstream from the mouth. This divided the domain conceptually into three different regions: the shelf, the estuary, and the (tidal) river (Figure 1). Of these regions, the portion of the estuary that remained after implementing an estuarine dam was focused on as the region of interest (ROI) in this study.

With respect to domain discretization, the horizontal size of the domain grid was 242 $\times$ 62 points, and the model was implemented with 20 vertical layers. After implementing the estuarine dam, the horizontal grid size was reduced to 66 $\times$ 62 points. The along-channel, across-channel, and vertical resolutions were nominally 0.5 km, 0.02 km, and 0.5 m, respectively. The model was run with a 10 second baroclinic time step, which was divided into 20 barotropic time steps, and the output was saved at 30-minute intervals.

Table 2 lists the sediment size classes used in this study and their properties. Six size classes were used, and these were divided into two groups: a marine sediment group (sand_1, mud_1, and mud_2) and a fluvial sediment group (sand_2, mud_3, and mud_4). Although these two groups shared the same properties, the model was initialized with only marine sediments in the domain. The fluvial sediments were discharged from the river and estuarine dam to investigate the mixing of marine and fluvial sediments. The sediment sizes for each group were heuristically chosen to be 0.125 mm, 0.062 mm, and 0.031 mm corresponding to very fine sand, coarse silt, and medium silt, respectively, with the latter two size classes representing muds. The critical bed shear stress for erosion and the settling velocity for each size class were computed following Soulsby (1997). Porosity was based on data in Whitehouse et al. (2000). The COAWST default erosion rate was used, and it lies within typical measured values (Whitehouse et al., 2000). With respect to the sediment bed, the total bed thickness was 100 m. A thick bed was used to ensure effectively unlimited sediment supply from the bottom. Initially, the marine sediments were mixed evenly in the sediment bed.

The model settings of this study utilized the third-order upstream horizontal advection of 3D momentum, fourth-order centered vertical advection of momentum, and tracer advection using the higher-order spatial interpolation at the middle temporal level (HSIMT; Wu & Zhu, 2010). To parameterize turbulence, this study used the two-equation k- turbulence closure implemented using the generic length-scale equation (Umlauf & Burchard, 2003; Warner et al., 2005). For simplicity, a logarithmic drag formulation with a constant hydraulic bottom roughness of $z_0 = 5 \times 10^{-5}$ m was utilized (cf. Tarpley et al., 2019). This study included a scheme for wetting and drying. During calculations, the water level of each cell was compared with the critical minimum depth of 0.1 m to represent emerging tidal flats. During the pre- and post-dam model runs, the bed model was allowed to evolve, resulting in modeled morphodynamic change. And the SSC was included in the equation of state.

The boundary conditions were closed on the channel banks and river end. The ocean boundary was open and featured a Chapman implicit boundary condition for the free surface and a Flather condition for the 2D momentum. The free surface and 2D momentum boundary conditions in the ocean boundary were chosen such that tidal currents were calculated from the free surface using reduced physics. On the shelf a weak along-shore flow (0.05 m s^{-1}) was set to prevent the formation of a bulge of freshwater at the estuary mouth following Hetland and Geyer (2004). Radiation and nudging conditions were applied to the tracers such that they can radiate from the domain at the ocean boundary. On the river boundary, river discharge was imposed. For the pre-dam case, the discharge was constant. For the post-dam case, the discharge points were relocated to the estuarine dam, the new river boundary. There, the discharge was episodic. The discharge duration and timing were set to 3 hours during mid-ebb, and the discharge frequency was set to once every 3 days. Both the discharge duration and frequency were based on mean values from Geum River estuary, South Korea (Figueroa et al., 2020b), where data on estuarine dam operation was available. The discharges were limited to ebb in order to prevent the salt intrusion. For the post-dam case, there was no discharge when the dam was closed. When the dam was open, the discharged volume was the same as the pre-dam case, however, it was discharged on a much shorter timescale. For both pre- and post-dam cases, the SSC from the river was constant for simplicity at a value of 0.15 kg m^{-3}, which was based on data in Milliman and Farnsworth (2013).

Table 1. Statistics of 10 estuaries with estuarine dams.

River estuary	Longitude (DD)	Latitude (DD)	Construction start	Construction end	Pre-dam length (km)	Post-dam length (km)	Mouth width (km)	Construction dates, pre-dam length data source
East								
Fitzroy								
Geum								
Haringvliet-								
Maas								
Murray-								
Darling								
Nagara-								
Kiso								
Nakdong								
Petitcodiac								
Senegal								
Tees								
Vilaine								
mean						-		

Construction dates and pre-dam estuarine length data sources: 1 = Connell et al. (1981); 2 = Kim et al. (2006); 3 = Tönis et al. (2002); 4 = Murray-Darling Basin Authority (www.mdba.gov.au); 5 = Kamada et al. (2004); Takahashi (1997); 6 = Ryu and Chang (1979); 7 = van Proosdij et al. (2009); 8 = Barusseau et al. (1998); 9 = Kidd et al. (2017); 10 = Traini et al. (2015). Post-dam length and mouth width based on Landsat views (earthexplorer.usgs.gov).

Table 2. Sediment properties.

	sand_1/sand_2	mud_1/mud_3	mud_2/mud_4
Grain size (mm)	0.125	0.062	0.031
Density (kg m^{-3})	2650	2650	2650
Porosity (%)	70	70	70
Critical bed shear stress (N m^{-2})	0.13	0.11	0.08
Erosion rate (kg m^{-2} s^{-1})	5.0×10^{-4}	5.0×10^{-4}	5.0×10^{-4}
Settling velocity (mm s^{-1})	11.9	3.11	0.80

Marine sediments (sand_1, mud_1, and mud_2) were initially present in the estuary. Fluvial sediments (sand_2, mud_3, and mud_4) were discharge by the river or estuarine dam.

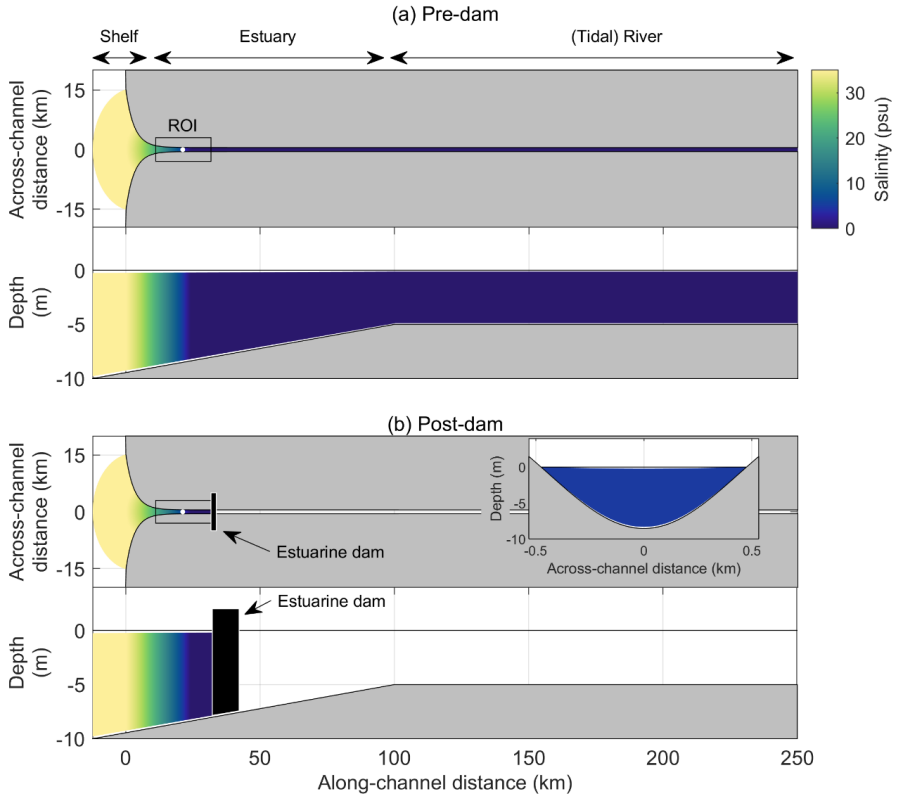

Figure 1. Pre-dam (a) and post-dam (b) model domain. Salinity and bathymetry are the model initial conditions. ROI is region of interest. Point is the ROI center, and is the location of the inset across-channel transect and the time series in Figure 4.

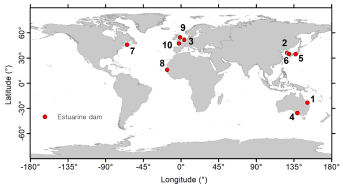

Figure 2. Location of selected estuaries with estuarine dams referred to in Table 1. Estuary IDs are: 1) East Fitzroy, 2) Geum, 3) Haringvliet-Maas, 4) Murray-Darling, 5) Nagara-Kiso, 6) Nakdong, 7) Petitcodiac, 8) Senegal, 9) Tees, 10) Vilaine.

2.1.3. Model scenarios

The model was run for four scenarios, each corresponding to a different estuarine type: 1) strongly stratified, 2) partially mixed, 3) periodically stratified, and 4) well-mixed estuaries. Each scenario consisted of three consecutive runs: a salinity initialization run, a pre-dam run, and a post-dam run. The salinity initialization run was initialized with a still water free surface, zero initial momentum, and an along channel salinity gradient (Figure 1). During the salinity initialization run, no sediment modules were activated. The run was forced by spring tides until it reached a periodic steady state. Subsequently, the pre-dam run was carried out using the output salinity field. With the appropriate initial salinity, the pre-dam runs were then carried out with the sediment modules activated. The sediment initial conditions were marine sediments well mixed in the bed and zero SSC in the water column. The pre-dam runs were forced by spring-neap cycles which lasted for 365 days. The spring-neap cycles were produced using two tidal constituents, the M_2 and S_2 constituents, and the amplitudes were weighted three to one as was done in Mellor (1996). A spring-neap cycle at the end of the pre-dam run was then used to represent the pre-dam estuary condition. Then, the salinity, bed morphology, SSC, and so forth were used as the initial condition for the post-dam runs. In these runs, the estuarine dam was placed. These runs were carried out for an additional 365 days, and a spring-neap cycle at the end of the post-dam run was used to represent the post-dam estuary condition.

The four scenarios were achieved by specifying the tidal range and the river freshwater volume discharge. To obtain the appropriate values needed to determine the estuary type, the estuarine parameter space (Geyer & MacCready, 2014) was utilized (Figure 3a). The estuarine parameter space is based on the Freshwater Froude number, Fr_f, and the mixing number, M, defined as (Geyer & MacCready, 2014):

$$Fr_f = \frac{U_R}{(\,\mathrm{g}S_{\mathrm{ocean}}H)^{\frac{1}{2}}} \quad (1a)$$

$$M^2 = \frac{C_D U_T^2}{\omega N_0 H^2} \quad (1b)$$

where $U_R = V/A$ is the cross-sectionally averaged river discharge velocity (m s^{-1}), V is the river volume flux (m^3 s^{-1}), A is the channel cross-sectional area (m^2), H is the cross-sectionally averaged depth (m), U_T is the amplitude of the cross-sectionally averaged tidal velocity (m s^{-1}), $N_0 = (\,gS_{ocean}/H)^{1/2}$ is the buoyancy frequency for maximum bottom-to-top salinity variation in an estuary (s^{-1}), $= 7.7 \times 10^{-4}$ psu^{-1} is the coefficient of haline contraction, $S_{ocean} = 35$ psu is the ocean salinity, $g = 9.8$ m s^{-2} is the acceleration due to gravity, C_D (taken here for simplicity as $C_D = 2.5 \times 10^{-3}$) is the drag coefficient, and $= 1.4 \times 10^{-4}$ s^{-1} is the tidal frequency. In Geyer and MacCready (2014), H and U_T are defined as a depth and the amplitude of the depth-averaged tidal velocity, respectively. These parameters can be defined using cross-sectional values (P. MacCready, personal communication). Therefore, in this study, H and U_T are defined as cross-sectionally averaged values, not their value at the channel thalweg. Physically, Fr_f is the net velocity of the river flow scaled by the maximum possible frontal propagation speed, and M is the ratio of tidal timescale to the mixing timescale (Geyer & MacCready, 2014).

To model the four different estuary types (i.e., strongly stratified, partially mixed, periodically stratified, and well-mixed), the factors other than U_R and U_T were taken as constant. Then, the types were defined based on U_R and U_T. U_R and U_T were set by specifying the river volume flux, V, and the amplitude of the tides on the shelf, respectively. U_T was directly proportional to the tidal amplitude on the shelf, and the appropriate tidal amplitude to generate the sought U_T was achieved by trial and error. The four model scenarios with their tidal range and their river and estuarine dam freshwater volume fluxes are summarized in Table 3.

Table 3. Model scenarios.

Scenario	**Estuarine type**	**Estuarine dam**	**Tidal range (m)**	**River/Estuarine dam freshwater volume flux (m^3 s^{-1})**
	Strongly stratified	Pre-dam		(steady)

Scenario	**Estuarine type**	**Estuarine dam**	**Tidal range (m)**	**River/Estuarine dam freshwater volume flux (m^3 s^{-1})**
		Post-dam		(dam closed), 7200 (dam open)
	Partially mixed	Pre-dam		(steady)
		Post-dam		(dam closed), 960 (dam open)
	Periodically stratified	Pre-dam		(steady)
		Post-dam		(dam closed), 720 (dam open)
	Well-mixed	Pre-dam		(steady)
		Post-dam		(dam closed), 48 (dam open)

Note: tidal range is at the shelf boundary.

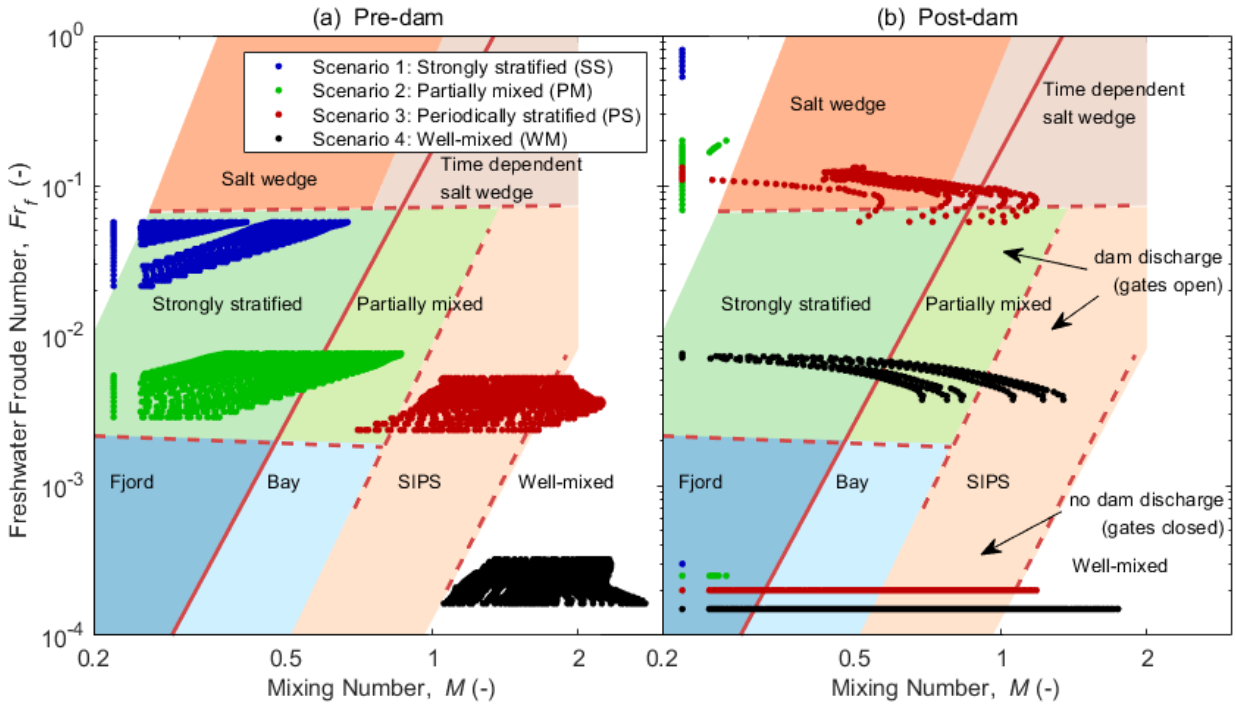

Figure 3. The estuarine parameter space for (a) pre-dam and (b) post-dam. Data points correspond to the region of interest (ROI) for each scenario. For data corresponding to no dam discharge, Fr_f was set to the minimum value of $Fr_f = 1.5 \times 10^{-4}$. To avoid overlap for these points, the scenarios were offset vertically from each other by $Fr_f = 0.5 \times 10^{-4}$ for clarity. Here SIPS is strain-induced periodically stratified estuary, also referred to simply as a periodically stratified estuary.

2.2. Data processing and analysis

2.2.1. Estuarine parameter space

The estuarine parameter space was used to analyze shifts in currents, stratification, and estuarine type due to the construction of an estuarine dam. For pre- and post-dam comparison, only points in the ROI over the representative spring-neap cycles were analyzed. Individual points were plotted to show the dynamic character of variation in the estuarine parameter space. Each point represents a classification based on cross-sectionally averaged depth, cross-sectional area, cross-sectionally averaged tidal current amplitude, and river volume flux from a tidal cycle at an across-channel transect. It occurred in some cases that the estuarine dam caused the tidal currents, and therefore the mixing number to be very low. At the same time, when the dam is closed, the river volume flux is $V = 0$ m^3 s^{-1}. In these cases, minimum values were heuristically specified in

order to keep the points within the estuarine parameter space, a log-log space where points with a zero coordinate are not typically plotted. The minimum values used in this study were $M = 0.22$, and $Fr_f = 1.5 \times 10^{-4}$. Physically, these represent very low currents and very low freshwater discharge, respectively.

2.2.2. Change in bed level and surficial sediment grain size

The impact of the estuarine dam on the estuarine depth and surficial sediment grain size was of interest for understanding changes in the sedimentary environment. To quantify these, their spring-neap average values for the pre- and post-dam cases were computed in the ROI. For depth change, the differences in pre- and post-dam bed level were computed, and a spatial average of this change over the ROI was also taken. In this way, areas that underwent erosion or deposition were visualized and the net impact could be seen. A similar procedure was carried out to quantify the change in the surficial sediment grain size. However, instead of comparing depths, the percent mud of the surface layer was computed by summing the marine and fluvial muds (i.e., mud_1, mud_2, mud_3, and mud_4), and it was this percent mud that was compared. In this way, areas that became sandier or muddier were visualized, and the net impact could be seen by spatially averaging over the ROI.

2.2.3. Sediment flux decomposition

This study aims at understanding the impact of an estuarine dam on the sediment accumulation and the estuarine turbidity maximum (ETM). Sediment accumulation and ETM formation are due to the convergence of tidally averaged, cross-sectionally integrated suspended sediment transport, $\left\langle A\,[\mathrm{uc}]_A \right\rangle$ (kg s^{-1}). To highlight the relevant underlying processes, the sediment fluxes were decomposed following Burchard et al. (2018) to gain insight into the processes:

$$\left\langle A\,[\mathrm{uc}]_A \right\rangle = \underset{T}{W\left[\langle D[\mathrm{uc}]_z\rangle\right]_y} = \underset{T_a}{W[\langle D\rangle\langle [u]_z\rangle\langle [c]_z\rangle]_y} + \underset{T_b}{W\left[\langle D\rangle\langle [u]'_z[c]'_z\rangle\right]_y} + \underset{T_c}{W\left[\langle D\rangle[\langle \tilde{u}\rangle\langle \tilde{c}\rangle]_z\right]_y}$$

$$+ \underset{T_d}{W\left[\langle D\rangle[\langle \tilde{u}'\tilde{c}'\rangle]_z\right]_y} + \underset{T_e}{W\left[\left\langle D'[\mathrm{uc}]'_z\right\rangle\right]_y} \quad (2)$$

where u is the along-channel current velocity (m s^{-1}), c is the suspended sediment concentration (sum of concentrations of all sediment size classes; kg m^{-3}), D is the depth (m), W is the width (m), and A is the cross-sectional area (m^2). Here, $[\,\cdot\,]_\mathrm{y}$, $[\,\cdot\,]_\mathrm{z}$, and $[\,\cdot\,]_\mathrm{A}$ denote lateral, vertical, and cross-sectional averages, respectively, and $\langle\bullet\rangle$ denotes a tidal average. The prime (') denotes the deviation from a tidal average and a tilde (~) denotes the deviation from a vertical mean. In this way the temporally averaged, cross-sectionally integrated transport was decomposed into five terms, T_a - T_e. Each term is associated with a different sediment transport mechanism. T_a is the transport by averages due to down-estuary river runoff. T_b is the tidal covariance transport due to tidal pumping.

T_c is the vertical covariance of tidal averages transport due to the estuarine exchange flow. T_d is the combined vertical and temporal covariance transport due to tidal straining. And T_e is the temporal depth covariance transport due to Stokes transport.

The terms were quantified along-channel in both the pre- and post-dam cases to understand the impact of the estuarine dam on the sediment flux mechanisms. As Equation 2 is exact only for constant depth or averaging in depth-proportional sigma coordinates (Burchard et al., 2018), averaging was done in sigma coordinates. The operations $\langle \bullet \rangle$ for a tidal average and (') for a deviation from a tidal average were computed using Lanczos 36-hour low-pass and high-pass filters, respectively. All the five sediment flux mechanisms have lateral and temporal variations due to channel-shoal bathymetry and the spring-neap cycle, respectively. These variations are beyond the scope of the present study, and therefore, T_a - T_e were averaged over the representative pre- and post-dam spring-neap cycles. This turned them into a function of only along-channel position.

3. Results

3.1. Pre- and post-dam time series of tide, current velocity, salinity, and SSC

Figure 4 shows time series at the center of the ROI for the strongly stratified (hereinafter SS; Figure 4a), partially mixed (hereinafter PM; Figure 4b), periodically stratified (hereinafter PS; Figure 4c), and well-mixed estuaries (hereinafter WM; Figure 4d). Pre- and post-dam tide (m), surface and bottom current velocity (m s^{-1}), surface and bottom salinity (psu), and bottom SSC (kg m^{-3}) are shown for each scenario. In terms of tide, the pre-dam tides of the spring-neap cycle increased from SS to WM cases. For the post-dam estuaries, the tides behaved differently. The SS estuary exhibited notable water level fluctuations after freshwater discharges. In other estuaries, the tides were amplified, most notably in the PS and WM estuaries.

The tidal currents varied in character and response to the estuarine dam. In the pre-dam estuaries, the current velocities increased from SS to WM similar to the tides. In the pre-dam SS estuary, there was a significant difference in the bottom and surface layers because it was a two layered system. The bottom layer tended to be landward and the surface layer seaward, but both fluctuated due to the tides, with the surface layer maintaining a unidirectional seaward flow while the bottom layer was bidirectional. In comparison, the PM, PS, and WM estuaries had bidirectional currents in both the bottom and surface layers. Vertical shear was indicated by differences in the bottom and surface currents. Both the PM and notably the PS estuaries showed stronger shear during ebbs. The post-dam SS estuary exhibited pulses of unidirectional flow > 2 m s^{-1} seaward. The initial pulse then exhibited oscillations and a strong vertical two-layer circulation until the discharge effect subsided and the currents became very weak until the next discharge pulse. The post-dam PM estuary showed reduced currents and a brief

two-layer circulation with each discharge. The post-dam PS and WM estuaries had significantly reduced currents compared to the pre-dam case. These cases did not exhibit the seaward pulses. For the PS estuary, however, the discharges were associated with irregular variations of vertical current shear.

The salinities also varied in character and response to the estuarine dam. As expected, the vertical stratification decreased from the SS to the WM case. The SS estuary bottom layer was always of marine salinity with the surface showing tidal variations and a water column stratification of about 25 psu. The PM estuary showed more tidal variations of bottom and surface salinity. The stratification was about 10 psu, and the stratification showed a spring-neap cycle with the least stratification after the spring tides. The PS estuary was periodically stratified during the neap tides but became more well mixed during the spring tides. During neap tide, the flood stratification was less at nominally 3 psu, whereas ebb stratification was more at nominally 8 psu. The pre-dam WM estuary showed negligible stratification and a water column salinity of about 32 psu.

The post-dam salinities were significantly different than the pre-dam salinities for all scenarios. The typical feature of post-dam salinities was an abrupt drop in salinity due to the freshwater discharge followed by a salinity recovery due to mixing. The SS and PM estuaries no longer showed significant spring-neap cycles in salinity. The PS estuary continued to show the spring-neap cycle in salinity. However, the semidiurnal tidal signal, particularly in the bottom layer was muted. The WM estuary indicated a slight reduction of salinity and periodic stratification of about $1 - 2$ psu. A notable feature was that the SS case salinity became fully fresh in the surface and the discharge affected even the bottom salinity at the center of the ROI. Another notable feature was the periodic stratification that occurred after the dam discharge in the PS estuary and to a lesser extent in the WM estuary. The post-dam periodic stratification occurred during spring tides but not neaps. Even though the pre- and post-dam PS estuary showed periodic stratification, the character of these two were different, particularly because in the post-dam case, the bottom salinity varied minimally in contrast to the pre-dam case bottom salinity.

The SSCs varied over orders of magnitude depending on the scenario, and there was a clear trend in the behavior of the pre- and post-dam SSC. The pre-dam spring tide bottom SSCs increased from 10^{-2} kg m^{-3} in the SS estuary to 10^{0} kg m^{-3} in the WM estuary. The pre-dam SSCs followed the spring-neap cycle. At the central point in the ROI, the SSC was due entirely to marine sediment (sand_1, mud_1, mud_2) in all scenarios. The post-dam estuaries showed different responses to the estuarine dam. The post-dam SSC increased for the SS estuary and decreased for the PM, PS, and WM estuaries. The signal of the spring-neap cycle in the SSC was eliminated from the SS and PM estuaries. And at the central point in the ROI in the post-dam SS estuary, SSC due to fluvial sediment (sand_2, mud_3, mud_4) occurred.

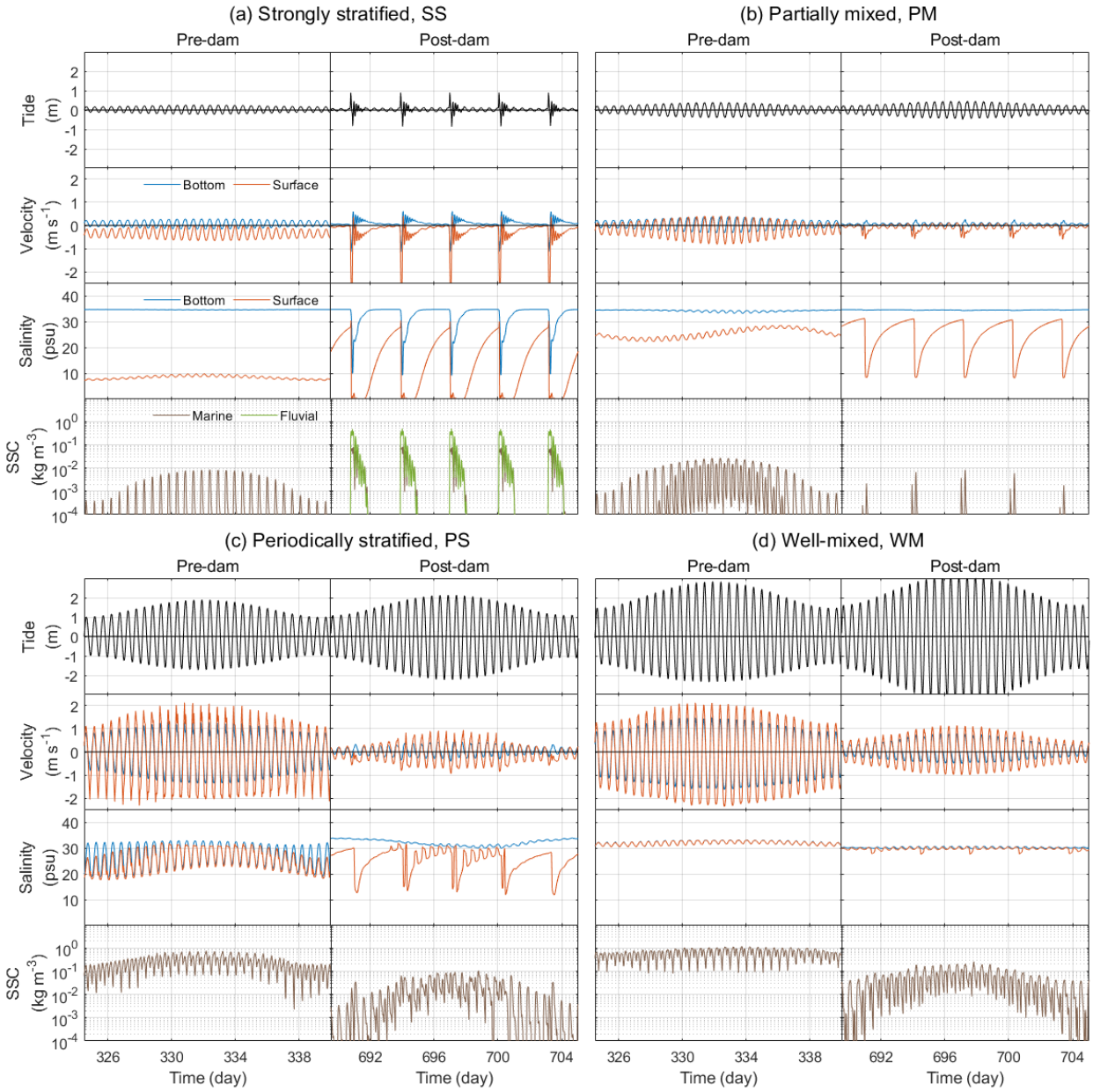

Figure 4. Pre- and post-dam time series for (a) strongly stratified, (b) partially mixed, (c) periodically stratified, and (d) well-mixed estuaries. For each is shown tide (m), bottom and surface along-channel velocity (m s^{-1}), bottom and surface salinity (psu), and suspended sediment concentration (SSC; kg m^{-3}). Time is day since initialization, with the estuarine dam placed on day 365.

Positive velocity is landward, negative velocity is seaward.

3.2. Change in along-channel profiles of tide, current velocity, salinity, and SSC

Figure 5 depicts the along-channel variation of the max tide (m), max current velocity (m s^{-1}), bottom and surface salinity (psu), and depth-averaged SSC (kg m^{-3}) averaged over the spring-neap cycle. The tide in the pre-dam estuaries was overall decreasing landward. In contrast, the tide in the post-dam estuaries increased toward the estuarine dam. The along-channel max depth-averaged current velocities were relatively constant at around 0.5 m s^{-1} in the pre-dam SS and PM estuaries, but showed peaks at around $x = 25$ km of 2.0 m s^{-1} and 2.5 m s^{-1} in the pre-dam PS and WM estuaries, respectively. The post-dam SS estuary showed an increase in currents up to 2.0 m s^{-1} adjacent to the dam. In contrast, the post-dam PM, PS, and WM estuaries exhibited a significant decrease in currents.

The pre-dam bottom and surface along-channel salinities increased with distance from the river with the maximum stratification in the middle of the fresh and marine salinity end members. The salt intrusion increased from $x = 80$ km in the pre-dam SS estuary, to $x = 200$ km in the pre-dam WM estuary. In the post-dam SS, PM and WM estuaries, the spring-neap averaged salinities were similar despite showing considerable differences in steadiness (Figure 4a and 4b salinity). The post-dam PS estuary showed a notable increase in the vertical salinity stratification.

The pre-dam SSC increased in magnitude from the SS to the WM scenario. In the SS and PM scenarios, there was a peak around $x = 100$ km because the model initial bathymetry had a depth transition there (Figure 1). The SSC was low in the pre-dam SS and PM estuaries at around 10^{-3} kg m^{-3}. In contrast, the pre-dam PS and WM estuaries reached depth-averaged SSCs on the order of 10^{-1} kg m^{-3}. No distinct ETM occurred in the SS and PM estuaries except at $x = 100$ km. In the PS and WM estuaries, there was an ETM around $x = 50$ km. In all pre-dam cases, the SSC in the estuary was associated with marine sediments except for the areas adjacent to the river source at $x = 250$ km, where SSC was due to fluvial sediments. In the post-dam estuaries, the SSC increased in the SS estuary to 10^{-2} kg m^{-3}. In the post-dam PM, PS, and WM estuaries the SSC decreased. In the post-dam PM case, the SSC reduced significantly after the dam. In the post-dam PS and WM cases, the ETM shifted to seaward of the dam and the SSC adjacent to the dam was characterized by lower concentration. In the PM, PS, and WM estuaries, SSC due to fluvial sediment was found only adjacent to the estuarine dam and appeared to quickly reduce with distance. In contrast to the pre-dam estuaries, the post-dam estuaries exhibited an increase in fluvial sediments in the ROI.

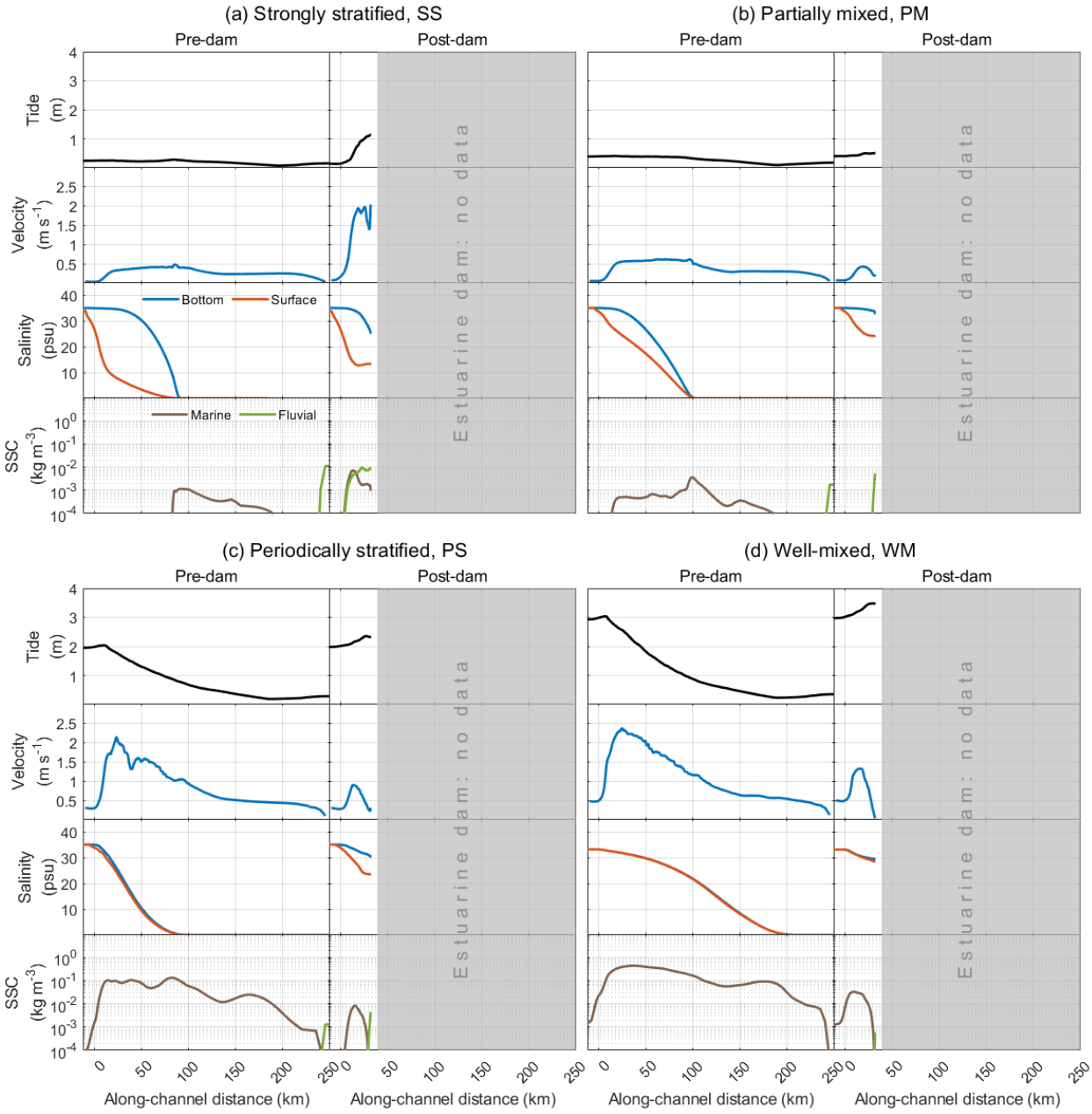

Figure 5. Pre- and post-dam along-channel profiles for (a) strongly stratified, (b) partially mixed, (c) periodically stratified, and (d) well-mixed estuaries. For each is shown the maximum tide (m), the maximum absolute along-channel velocity (m s^{-1}), spring-neap averaged bottom and surface salinity (psu), and spring-neap and depth averaged suspended sediment concentration (SSC; kg

m^{-3}). Along-channel distance is distance from the widest point in the domain. Positive is landward and goes through the shelf, estuary, and (tidal) river.

3.3. Shifts in the estuarine parameter space

Figure 3 shows the shift in estuarine type from the pre- to post-dam estuaries. For a given scenario, variation of M corresponded to changes in the current magnitude due to the spring-neap cycle, while variation of the Fr_f corresponded to changes in along-channel position, where deeper sections (larger cross-sectional areas) had smaller Fr_f. Figure 3a shows that after approximately one year, the estuaries remained in the part of the parameter space for which they were designed. It can be noted that the PM estuary fell into the strongly stratified estuary type during neap tides but was partially mixed during spring tides. Figure 4 supports that the scenarios' pre-dam estuary conditions matched their intended estuarine types.

The post-dam estuarine types were significantly different from the pre-dam estuarine types for all scenarios (Figure 3b). In this figure, while the ROI points occupied a relatively small space for the pre-dam cases, the post-dam points were spread out over the estuarine parameter space. The post-dam points formed two clusters. The first cluster was at relatively low mixing numbers (predominantly $M < 1$) and relatively high freshwater Froude numbers (Fr_f 10^{-3} – 10^{-0}). These corresponded to the times of estuarine dam freshwater discharge with a large Fr_f. At the same time, M was relatively small due to the weaker tidal currents in the post-dam estuaries. The second cluster was at relatively low mixing numbers (predominantly $M < 1$) and low freshwater Froude numbers ($Fr_f < 10^{-3}$). These corresponded to the times of no freshwater discharge. Fr_f therefore was set to the minimum value of $Fr_f = 1.5 \times 10^{-4}$. Yet it should be noted that for the second cluster, the scenarios were offset vertically from each other by $Fr_f = 0.5 \times 10^{-4}$ for clarity. Overall, post-dam estuaries were shifted to more stratified types during dam discharge (salt wedge, strongly stratified, or partially mixed). During no dam discharge, the post-dam estuaries shifted to types with weak river forcing (fjord, bay, or periodically stratified/SIPS).

3.4. Bathymetric and surficial mud content maps

Figure 6 shows the pre- and post-dam depths after approximately 1 year of morphodynamic evolution from the initial bathymetry (for the pre-dam cases) or from the pre-dam cases' bathymetry (for the post-dam cases). The initial bathymetry relative to mean sea level in the ROI had a depth of 8.50 m in the channel thalweg and an elevation of 1.50 m on the channel banks. At the end of the pre-dam runs, the thalweg depths ranged from 8.50 – 12.42 m, and the elevation of the banks ranged from 1.50 – 1.64 m. This indicated that the thalweg tended to deepen, and the banks tended to aggrade. Overall, the pre-dam SS and PM estuaries showed the least morphodynamic change (Figure 6a and 6b, pre-dam), while the pre-dam PS and WM estuaries showed more morphodynamic change (Figure 6c and 6d, pre-dam). In addition to deposition on the banks, a mouth bar deposit and channel bifurcation developed in the

pre-dam WM estuary. The post-dam estuarine depths were similar to those of the pre-dam estuaries. An exception was the post-dam SS estuary (Figure 6a, post-dam), where the estuary dam discharge generated a scour hole. The scour resulted in a depth change from a pre-dam depth of 8.09 m to a post-dam depth of 11.06 m for the area adjacent to the estuarine dam. These scoured sediments were then deposited further seaward.

The bed level changes (post-dam bed level minus pre-dam bed level) are also shown in Figure 6, with the color bar limited to $\pm$ 1 m of bed level change for clarity. The greatest morphological change due to the estuarine dam occurred for the strong river forcing (SS estuary) and strong tide forcing (WM estuary) scenarios. For the SS estuary, the greatest bed level change was 2.97 m of erosion due to bed scour adjacent to the estuarine dam (Figure 6a, bed level change). For the WM estuary, the greatest depth change was 1.08 m of deposition in the channel of the post-dam WM estuary (Figure 6d, bed level). The PM and PS bed level changes were intermediate between the SS and WM scenarios. The PM estuary bed level changes were characterized by deposition of sediment directly adjacent to the estuarine dam (Figure 6b, bed level change). This amounted to 0.75 m of deposition of fluvial sediments (Figure 4b, SSC). The bed level change in the PS estuary mainly featured erosion along the thalweg. Overall, the SS and PS estuaries showed erosion of 0.007 m and 0.019 m, respectively, and the PM and WM estuaries showed deposition of 0.017 m and 0.003 m, respectively. The absolute bed level change affected by the estuarine dam increased from the SS estuary to the PS estuary, and then decreased for the WM estuary.

Figure 7 shows the pre- and post-dam surface mud content and surface mud content change after approximately one year of hydrodynamic sorting from the initial poorly sorted bed (for the pre-dam cases) or from the pre-dam cases' bed (for the post-dam cases). In contrast to the depth and bed level changes, the surface mud content showed less variation between the scenarios. The beds of the pre-dam estuaries were hydrodynamically sorted such that there was almost no mud (0%) in the channel but the adjacent banks tended to have higher surface mud contents. The surface mud content of the banks increased up to 100% for the pre-dam WM scenario (Figure 7d). The shelf areas also became hydrodynamically sorted with higher mud contents in the PS and WM scenarios (Figure 7c and 7d). The post-dam estuaries responded to the estuarine dam generally by shifting to higher surface mud contents (Figure 7, post-dam). For the post-dam PS and WM estuaries, the increase in the mud content of the ROI was accompanied by a decrease in the mud content of the shelf (Figure 7c and 7d, surface mud change). On the other hand, the surface mud content increased on the shelf to 100% in the post-dam SS estuary (Figure 7a, post-dam and surface mud % change). Overall, all scenarios showed a positive surface mud change in the ROI, ranging over a 12.2 – 22.4% increase, indicating the post-dam estuaries were muddier than their pre-dam counterparts.

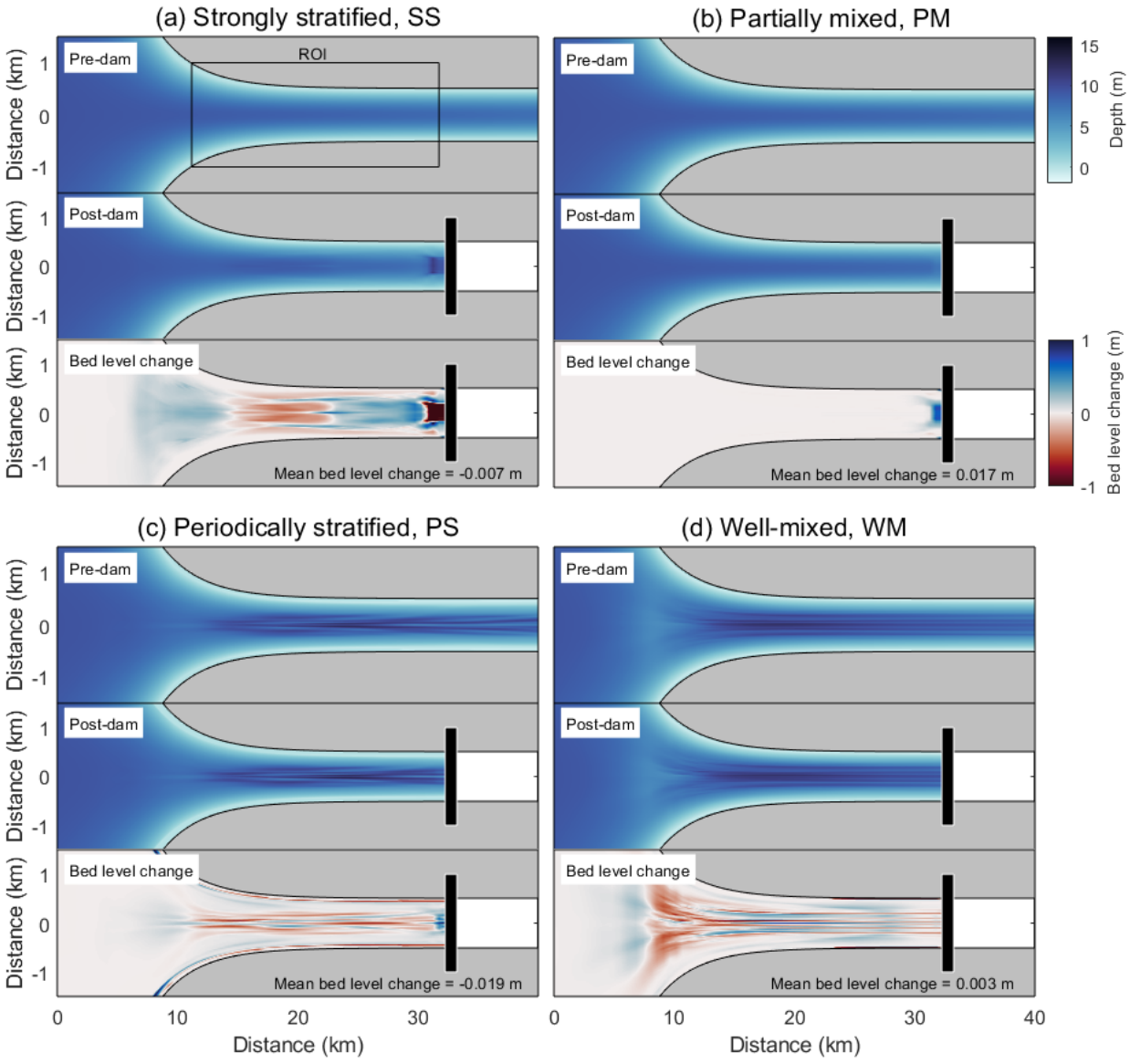

Figure 6. Pre- and post-dam depth and bed level change maps for (a) strongly stratified, (b) partially mixed, (c) periodically stratified, and (d) well-mixed estuaries. For each is shown the pre- and post-dam depth (m) and the bed level change (post-dam bed level minus pre-dam bed level; m). ROI is the region of interest. Positive bed level change is deposition, and negative bed level change is erosion. The areal mean bed level change for the ROI is written for each scenario.

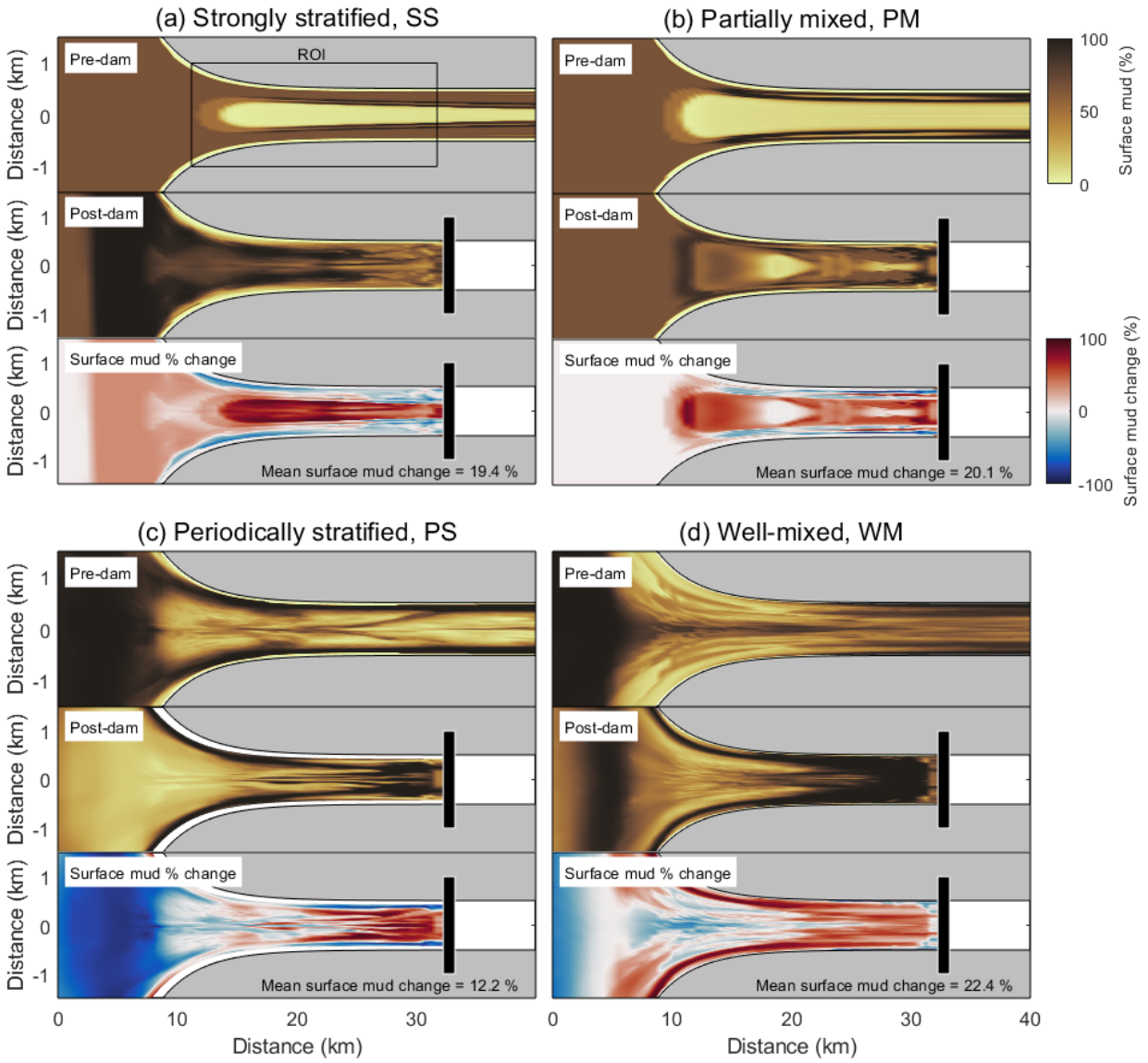

Figure 7. Pre- and post-dam surface mud content and surface mud content change maps for (a) strongly stratified, (b) partially mixed, (c) periodically stratified, and (d) well-mixed estuaries. For each is shown the pre- and post-dam surface mud content (%) and the surface mud content change (post-dam surface mud content minus pre-dam surface mud content; %). ROI is the region of interest. Positive surface mud content change is becoming muddier, and negative surface mud content change is becoming sandier. The surface mud content change of -100% denotes an area of pure mud converted to pure sand,

and a change of 100% denotes an area of pure sand converted to pure mud. The areal mean surface mud content change for the ROI is written for each scenario.

3.5. Along-channel decomposed sediment fluxes

Figure 8 presents the spring-neap averaged, cross-sectionally integrated sediment flux (kg s^{-1}) along-channel profiles for each scenario. Both the pre- and post-dam cases are decomposed into the five sediment flux mechanisms. The pre-dam cases differed amongst the scenarios in terms of the sediment flux magnitudes, the spatial along-channel structure of the sediment flux mechanisms, and the relative importance of the sediment flux mechanisms (Figure 8, pre-dam decomposed). The magnitude of the sediment flux increased from the pre-dam SS estuary (order of 10^{-2} kg s^{-1}) to the pre-dam WM estuary (order of 10^{2} kg s^{-1}). In general, there was a peak in sediment fluxes in the estuary. This peak tended to move seaward from the SS to the WM estuary.

For the pre-dam estuaries, the river runoff, T_a, increased in relative importance from the SS to the WM estuary. The river runoff was always directed seaward. Tidal pumping, T_b, was of primary importance in all pre-dam estuaries. While it was directed landward in the pre-dam SS and PM estuaries, it was directed seaward in the pre-dam PS and WM estuaries. The estuarine exchange flow, T_c, was of primary importance in the SS and PM estuaries. It was always positive and reached a maximum magnitude in the PM estuary. T_c was negligible in the pre-dam PS and WM estuaries. Tidal straining, T_d, was of secondary importance in the SS and PM estuaries and was negligible in the PS and WM estuaries. In the pre-dam SS and PM estuaries, T_d was directed seaward. The Stokes transport, T_e, which was negligible in the pre-dam SS estuary, became increasingly important from the PM to the WM estuary. The Stokes transport was always directed landward.

For the post-dam estuaries (Figure 8, post-dam, decomposed), each scenario showed changes in the sediment flux magnitudes, the spatial along-channel structure of the sediment flux mechanisms, and the relative importance of the sediment flux mechanisms. For the post-dam SS estuary, the post-dam sediment flux magnitude increased, while the sediment flux magnitudes decreased for the post-dam PM, PS, and WM estuaries. The spatial along-channel structure of the sediment flux mechanisms depended on each scenario. For the post-dam SS estuary, the sediment flux mechanisms shifted seaward to the shelf. For the post-dam PM estuary, the sediment fluxes were greatest adjacent to the estuarine dam and decreased rapidly seaward.

For the post-dam estuaries, T_a increased in relative importance in the post-dam SS estuary, but decreased for the post-dam PM, PS, and WM estuaries. Remaining of primary importance, T_b changed in direction from landward to seaward for the post-dam SS and PM estuaries, and from seaward to landward for the post-dam PS and WM estuaries. T_c tended to decrease for the post-dam SS and PM estuaries but increased for the post-dam PS and WM estuaries. T_d remained a small sediment flux mechanism and negligible in the post-dam

estuaries. T_e decreased for all post-dam estuaries. Only in the post-dam WM estuary did this mechanism remain non-negligible.

Figure 8 also depicts the pre- and post-dam total sediment fluxes ($T_{pre\text{-}dam}$ and $T_{post\text{-}dam}$; pre- & post-dam, total). In the pre-dam SS and PM estuaries, the total sediment fluxes were directed landward, whereas in the pre-dam PS and WM estuaries, they were directed seaward. The absolute value of the total sediment flux gradients increased from the pre-dam SS estuary to the pre-dam WM estuary. The gradients, or slopes, of the sediment flux were predominately negative in the ROI for the pre-dam SS and PM estuaries (denoting flux convergence), whereas they were positive in the pre-dam PS and WM estuaries (denoting flux divergence). The sediment fluxes switched direction in the post-dam estuaries. The absolute value of the gradients of the total sediment flux increased for the post-dam SS and PM estuaries and decreased for the post-dam PS and WM estuaries. For the post-dam SS estuary, there was a switch to a more complex along-channel sediment flux convergence-divergence-convergence. For the post-dam WM estuary, however, there was a switch from divergence to convergence.

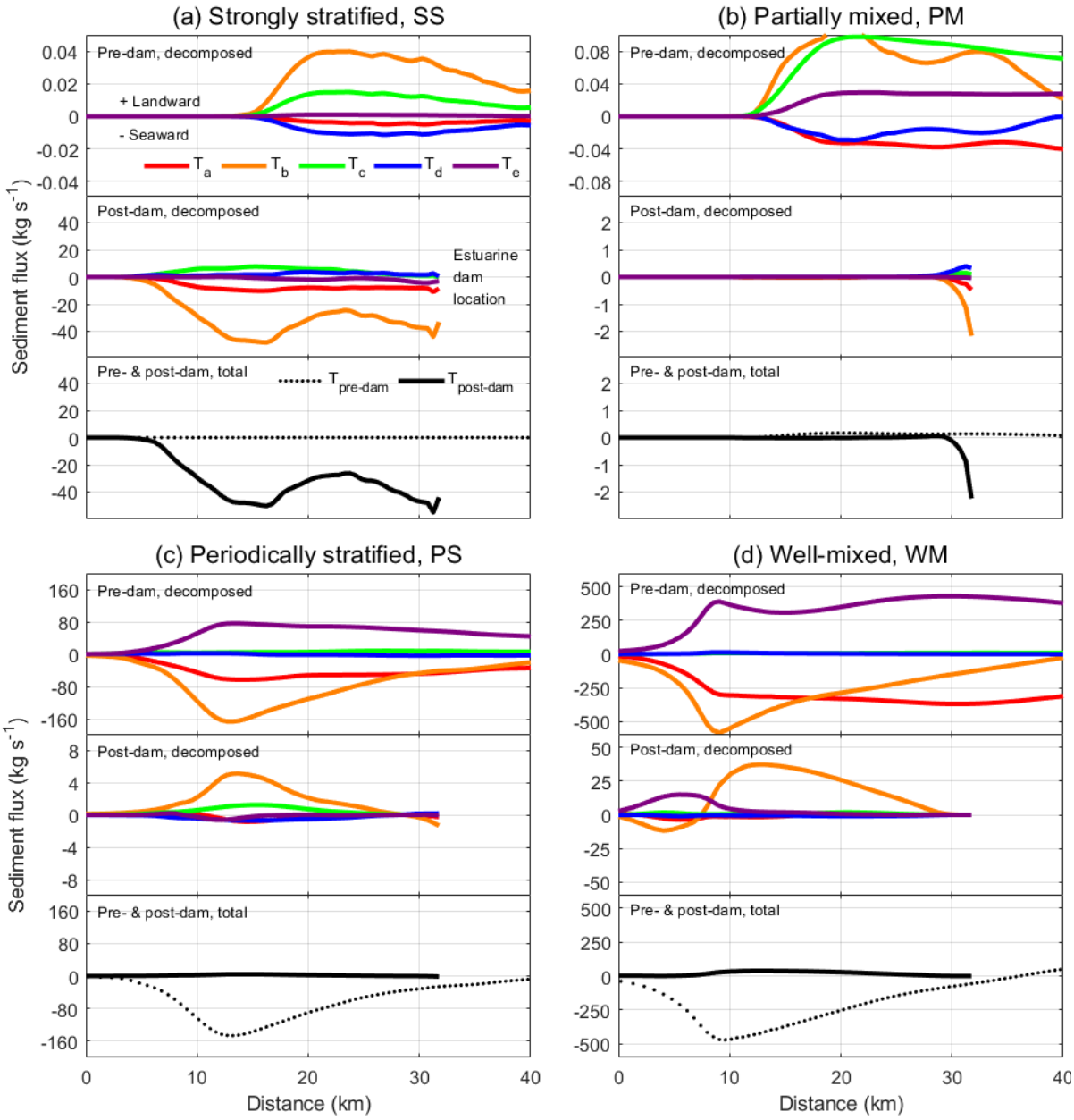

Figure 8. Pre- and post-dam spring-neap averaged, cross-sectionally integrated sediment fluxes profiles for (a) strongly stratified, (b) partially mixed, (c) periodically stratified, and (d) well-mixed estuaries. For each is shown the pre- and post-dam decomposed sediment fluxes (T_a, T_b, T_c, T_d, T_e; kg s^{-1}) and the pre- and post-dam total sediment fluxes ($T_{pre\text{-}dam}$, $T_{post\text{-}dam}$; kg s^{-1}). T_a is river

runoff, T_b is tidal pumping, T_c is estuarine exchange flow, T_d is tidal straining, and T_e is Stokes transport. Along-channel distance is distance from the widest point in the domain. Positive is landward and goes through the shelf to the estuary, including the region of interest (ROI, location of post-dam estuary). Note the y-axis limits vary orders of magnitude amongst a, b, c, and d.

4. Discussion

4.1. Impact of estuarine dams on estuarine hydrodynamics and sedimentary environment

This study has provided new insight into how estuarine dams affect tidal currents, stratification, estuarine type, SSC, bed level, surficial grain size, the abundance of fluvial sediment, and the sediment flux mechanisms for a range of estuarine types. This section will discuss changes which were common to all estuarine types as well as changes which depended on the estuarine type.

All scenarios investigated in this study were affected by two main changes induced by the estuarine dam. First was the physical shortening of the estuarine geometry. This relocated the tidal limit and ETM, reduced salt intrusion length, and resulted in a dead-end channel where currents vanished during no discharge periods (Figure 5). Second was the alteration of the estuarine tide and river forcing. Tidal currents were reduced due to the loss of the tidal prism, and the freshwater discharge switched from steady to unsteady (Figure 4). Reduction of the tidal currents resulted in a uniform decrease in the mixing number, M, while unsteady discharge resulted in alternating large and zero freshwater Froude number, Fr_f (Figure 3). Consequently, the post-dam estuaries tended to salt wedge and strongly stratified types during freshwater discharge, but during no freshwater discharge they became fjord, bay, or periodically stratified types based on the estuarine parameter space. Moreover, the reduction of tidal currents permitted the deposition of suspended sediment in addition to inputs of mud from the river and shelf. This resulted in an increase in surficial mud content in all scenarios (Figure 8). At the same time, all scenarios also exhibited an increase in fluvial sediment abundance due to the direct discharge of fluvial sediments to the ROI in the post-dam estuaries (Figure 5).

Comparison of the range of post-estuaries revealed that some responses of an estuary to an estuarine dam depended on the estuarine type. This study suggested the existence of two end members; one end member was the strong river case (SS estuary), and the other end member was the strong tide case (WM estuary). For the post-dam SS estuary, the water levels, currents, salinity, and SSC were dominated by the freshwater discharge from the estuarine dam (Figure 4). This was because the input of large volumes of freshwater rapidly generated significant barotropic pressure gradients, salinity fronts, and bed shear stresses. On the other hand, for the post-dam WM estuary, the water levels, currents, and SSC were dominated by changes in the tide due to tidal reflection, loss of tidal prism, and reduced bed shear stresses. The salinity indicated the potential to develop periodic stratification, but overall exhibited relatively minor changes

in magnitude (Figure 4). The development of periodic stratification was due to the relatively strong along-channel salinity gradient as the freshwater discharge from the estuarine dam interacts with the strong vertical shear of the tidal currents in the post-dam WM estuary.

Another difference from these end members was that the post-dam SS estuary indicated scour adjacent to the estuarine dam and a muddier shelf, whereas the post-dam WM estuary indicated reworking of a mouth bar deposit and a sandier shelf (Figures 7 and 8). For the post-dam SS estuary, bed scour in front of the estuarine dam occurred due to a shift in the river forcing to brief, high discharge events, resulting in significant bottom stress. At the same time, the freshwater river plume transported muddy fluvial sediments to the shelf, resulting in a muddier shelf. For the post-dam WM estuary, this was due to changes in the tidal characteristics induced by the estuarine dam, particularly the shift toward landward tidal asymmetry and bed shear stresses, which reworked shelf deposits and preferentially transported muds with a smaller critical bed shear stress for erosion into the post-dam estuary.

Analysis of the pre- and post-dam sediment fluxes revealed that the post-dam SS estuary exhibited an increase in the total sediment flux magnitude and the total sediment flux direction shifted from landward to seaward (Figure 9). This was due to the shift from a relatively low energy, stratified environment to a high energy environment characterized by seaward pulses, which extended through the entire water column. The change in the freshwater discharge decreased the steady horizontal salinity gradient and the associated landward sediment flux due to exchange flow, while it increased the seaward sediment flux due to river runoff. At the same time, the episodic, intratidal nature of the seaward runoff led to an increase in the seaward tidal covariance transport (tidal pumping). On the other hand, the post-dam WM estuary exhibited a decrease in the total sediment flux magnitude and the total sediment flux direction shifted from seaward to landward (Figure 9). In this case, the reduced tidal currents were responsible for the decrease in the total sediment flux magnitude. The seaward river runoff, which was a primary mechanism transporting sediment seaward in the pre-dam WM estuary, became negligible for the post-dam WM estuary. Although relatively small, the seaward river runoff of the pre-dam estuary extended throughout the well-mixed water column and could transport the high SSC steadily seaward. This steady, single layer river runoff was changed to an unsteady two-layer system in the post-dam WM estuary, which became negligible as a seaward sediment flux mechanism. At the same time, tides in shortened post-dam estuary behaved more like a standing wave due to reflection, resulting in the weakening of the landward Stokes transport and the change in the tidal asymmetry leading to landward tidal pumping.

4.2. Reliability of idealized estuary model

The idealized estuary model in this study agrees in several respects with existing field observations providing evidence that the model is reliable in capturing the main impacts of estuarine dams on estuaries. This includes tidal amplification of

several centimeters such as has been observed in the Guadalquivir estuary, Spain (Díez-Minguito et al., 2012), and Geum estuary, South Korea (Kwon and Lee, 1999). The idealized model also reproduced several cm s^{-1} reduction in the tidal currents such as has been observed in the Vilaine estuary, France (Traini et al., 2015). In addition, the model was able to capture the rapid shifts in estuarine type during discharge which has been observed by field observations in three estuaries with estuarine dams by Shin et al. (2019). Also the model agreed with the increase in surficial mud content which has been observed in sediment cores acquired in the Nakdong estuary, South Korea, where a sharp boundary between pre-dam sand facies and post-dam mud facies was identified (Williams et al., 2013). And, another point of agreement between the idealized model and field observations was the increased fluvial sediment abundance which has been recorded in the Yeongsan estuary, South Korea, based on organic matter stable isotope ratios and short-lived radioisotope geochronology (Williams et al., 2014).

The idealized estuary model was also able to reproduce sediment flux mechanisms in the pre-dam estuaries in accordance with field observations. This includes features such as that the river runoff is generally being directed seaward (Burchard et al., 2018), the exchange flow is important in partially mixed estuaries (Sommerfield and Wong, 2011), and tidal pumping (Geyer et al., 2001; Uncles et al., 1985) and Stokes transport (Moskalski et al., 2020) are generally more important in estuaries with moderate or strong tides. However, while previous studies have shown that tidal straining can be an important sediment flux mechanism in PS estuaries (Burchard et al., 2013; Scully and Friedrichs, 2007), it is noted that tidal straining was never a primary sediment flux mechanism in this study. This may have been due to the intricacy of specifying the relative freshwater discharge and tidal forcing while modeling a PS estuary.

The idealized estuary model also captured the main features of sediment flux mechanisms in post-dam estuaries, including the two end members. For example, the post-dam SS estuary in this study showed similarity with the microtidal Nakdong estuary, South Korea, during a strong discharge event (Chang et al., 2020; Williams et al., 2015). For both cases, the seaward river runoff sediment flux was a primary sediment flux mechanism. It can be noted that in this study the intratidal freshwater discharges also contributed to the seaward tidal covariance (tidal pumping) sediment flux mechanism. As another example, the post-dam WM estuary in this study showed similarity with the macrotidal Geum estuary, South Korea (Figueroa et al., 2020a, 2020b; Kim et al., 2006). For both cases, landward tidal pumping was the primary sediment flux mechanism.

4.3. Future issues regarding estuarine dams

This study is one of the first to investigate the effect of estuarine dams on a range of estuarine types. It provides evidence that estuarine dams are typically located relatively near the estuarine mouths (Table 1). At this distance, the tidal excursion can act as an important length scale for the sediment transport because the seaward sediment fluxes induced by episodic discharge are limited

to approximately a tidal excursion since freshwater discharge occurs during ebb tides to prevent salt intrusion (Figueroa et al., 2020b). Future research may further investigate the case where the estuarine dam location extends upstream and approaches the length scale of the tidal wave. In this case tidal barriers placed near the head may reduce tidal amplitudes. Generally, increases in tidal amplitudes are expected if a tidal barrier is located at nodes along the channel and decreases in tidal amplitudes are expected if a tidal barrier is located at the antinodes along the channel (Prandle and Rahman, 1980), and this has implications for the along channel sediment transport (e.g., Díez-Minguito et al., 2012).

Future research may also investigate the effect waves as well as the effect of discharge frequency, which depends on the climate of an estuary's watershed and the volume available for freshwater storage in the reservoir upstream of the estuarine dam. Field studies have clearly indicated that estuarine dams and their discharge frequency can impact the mouths of wave-dominated estuaries due to reducing bidirectional tidal currents and seaward river flushing. For example, estuarine dams constructed in wave-dominated estuaries have been observed to result in the formation of barrier islands (Williams et al., 2013), river mouth migration (Barusseau et al., 1998), and an increased likelihood of tidal inlet closure and the propensity for higher salinities in the adjacent lagoons (Webster, 2005).

5. Conclusions

The research questions for this study were, for a range of estuarine types: 1) how does an estuarine dam affect the tidal currents, stratification, and estuarine type?; 2) how does an estuarine dam affect the estuarine SSC, bed level, surficial grain size, and abundance of fluvial sediment?; and 3) how does an estuarine dam affect the estuarine sediment flux mechanisms? To address these questions, a hydrodynamic and sediment transport numerical model was applied to an idealized estuarine geometry over a range of estuarine types. These estuarine types formed four scenarios which included SS, PM, PS, and WM estuaries.

It was found that the estuarine dam physically shifted the tidal limit, salt intrusion, and ETM seaward. The estuarine dam caused several changes including tidal amplification, reduced tidal currents, changes in water column stratification, changes in SSC, muddier surficial grain sizes, and a greater presence of fluvial sediments. The key shifts in forcing were the uniformly reduced tidal currents and the switch from steady to unsteady river forcing. This led to a shift toward salt wedge and strongly stratified estuarine types during estuarine dam discharge and toward fjord, bay, and periodically stratified estuarine types during no discharge.

The shift in sediment flux mechanisms followed two end members, the SS estuary with strong river forcing and the WM estuary with strong tidal forcing. For the SS end member, there was a shift from landward estuarine exchange flow and tidal pumping to seaward river runoff and seaward tidal pumping

sediment flux mechanisms. For the WM end member, there was a shift from seaward river runoff and tidal pumping and landward Stokes transport to landward tidal pumping and Stokes transport sediment flux mechanisms. Therefore, the estuarine dam increased the seaward river runoff for cases with strong river and increased the landward tidal pumping for cases with strong tides.

1. **Acknowledgements**

This research was supported by Basic Science Research Program (2017R1D1A1B05033162)

and Center for Anthropocene Studies (2018R1A5A7025409) through the National Research Foundation of Korea (NRF). This work was also supported by the Ministry of Oceans

and Fisheries, Korea under the project titled "Establishment of the ocean research station in the jurisdiction zone and convergence research". The authors would like to acknowledge J.C. Warner for assistance during the preparation of the model grid, P. MacCready for clarification regarding the estuarine parameter space, and D. Ralston for assistance with the sediment flux decomposition.

Data Availability Statement

Based on FAIR, data will be uploaded to an online repository at a future stage of review of this manuscript.

References

https://doi.org/10.1016/S0899-5362(98)00014-1

https://doi.org/10.1175/1520-0485(1998)028%3C0309:TFOETM%3E2.0.CO;2

https://doi.org/10.1175/JPO-D-12-0231.1

https://doi.org/10.1146/annurev-marine-010816-060535

https://doi.org/10.1016/j.margeo.2020.106364

https://doi.org/10.1175/2009JPO4016.1

https://doi.org/10.1029/2011JC007344

https://doi.org/10.1016/j.margeo.2019.03.009

https://doi.org/10.1016/j.ecss.2020.106718

https://doi.org/10.1016/j.margeo.2020.106318

https://doi.org/10.1146/annurev-fluid-010313-141302

https://doi.org/10.1016/j.jcp.2007.06.016

https://doi.org/10.1175/JPO2646.1

https://doi.org/10.1029/2006JC003615

https://doi.org/10.3390/rs13020330

https://doi.org/10.1016/j.ocecoaman.2016.08.012

https://doi.org/10.1016/j.ecss.2006.03.003

https://doi.org/10.1016/j.ocecoaman.2012.05.010

https://doi.org/10.1175/1520-0485(1980)010%3C1552:TRIE%3E2.0.CO;2

https://doi.org/10.1139/anc-2018-0013

https://doi.org/10.3390/jmse7100334

https://doi.org/10.1016/S0378-3839(01)00026-6

https://doi.org/10.1016/j.ecss.2015.06.025

https://doi.org/10.1357/002224003322005087

https://doi.org/10.1016/j.csr.2015.08.009

https://doi.org/10.1016/j.ocemod.2010.07.010

https://doi.org/10.1029/2004JC002691

https://doi.org/10.1016/j.cageo.2008.02.012

https://doi.org/10.1016/j.margeo.2013.05.010

https://doi.org/10.1016/j.margeo.2014.08.004

https://doi.org/10.1016/j.margeo.2015.08.004

https://doi.org/10.1007/s10236-013-0662-9

https://doi.org/10.1016/j.ocemod.2009.12.001

Barusseau, J.P., Bă, M., Descamps, C., Diop, E.S., Diouf, B., Kane, A., Saos, J.L., & Soumare, A. (1998). Morphological and sedimentological changes in the Senegal River estuary after the constuction of the Diama dam. *Journal of African Earth Sciences*, 26(2), 317-326. Burchard, H., & Baumert, H. (1998). The formation of estuarine turbidity maxima due to density effects in the salt wedge: A hydrodynamic process study. *Journal of Physical Oceanography*, 28(2), 309-321. Burchard, H., Schuttelaars, H.M., & Geyer, W.R. (2013). Residual sediment fluxes in weakly-to-periodically stratified estuaries and tidal inlets. *Journal of Physical Oceanography*, 43(9), 1841-1861. Burchard, H., Schuttelaars, H.M., & Ralston, D.K. (2018). Sediment trapping in estuaries *Annual Review of Marine Science*, 10, 371-395. Chang, J., Lee, G., Harris, C.K., Song, Y., Figueroa, S.M., Schieder, N.W., & Lagamayo, K.D. (2020). Sediment transport mechanisms in altered depositional environments of the Anthropocene Nakdong Estuary: A numerical modeling study. *Marine Geology*, 430, 106364. Chen, S.N., & Sanford, L.P. (2009). Axial wind effects on stratification and longitudinal salt transport in an idealized, partially mixed estuary. *Journal of Physical Oceanography*, 39(8), 1905-1920. Connell, D.W., Bycroft, B.M., Miller, G.J., & Lather, P. (1981). Effects of a barrage on flushing and water quality in the Fitzroy River estuary, Queensland. *Marine and*

Freshwater Research, 32(1), 57-63. https://doi.org/10.1071/MF9810057Davis Jr, R.A. & Fitzgerald, D.M. (2020). Beaches and Coasts. John Wiley & Sons.Díez-Minguito, M., Baquerizo, A., Ortega-Sánchez, M., Navarro, G., & Losada, M. A. (2012). Tide transformation in the Guadalquivir estuary (SW Spain) and process-based zonation. *Journal of Geophysical Research: Oceans*, 117(C3). Figueroa, S.M., Lee, G., & Shin, H.J. (2019). The effect of periodic stratification on floc size distribution and its tidal and vertical variability: Geum Estuary, South Korea. *Marine Geology*, 412, 187–198. Figueroa, S.M., Lee, G., & Shin, H.J. (2020a). Effects of an estuarine dam on sediment flux mechanisms in a shallow, macrotidal estuary. *Estuarine, Coastal and Shelf Science*, 238, 106718. Figueroa, S.M., Lee, G., Chang, J., Schieder, N.W., Kim, K., & Kim, S.Y. (2020b). Evaluation of along-channel sediment flux gradients in an anthropocene estuary with an estuarine dam. *Marine Geology*, 429, 106318. Geyer, W.R., Woodruff, J.D., & Traykovski, P. (2001). Sediment transport and trapping in the Hudson River estuary, *Estuaries*, 24, 670-679. https://doi.org/10.2307/1352875Geyer, W.R., & MacCready, P. (2014). The estuarine circulation. *Annual Review of Fluid Mechanics*, 46, 175–197. Haidvogel, D.B., Arango, H., Budgell, W.P., Cornuelle, B.D., Curchitser, E., Di Lorenzo, E., Fennel, K., Geyer, W.R., Hermann, A.J., Lanerolle, L., & Levin, J. (2008). Ocean forecasting in terrain-following coordinates: Formulation and skill assessment of the Regional Ocean Modeling System. *Journal of Computational Physics*, 227(7), 3595-3624. Hetland, R.D., & Geyer, W.R. (2004). An idealized study of the structure of long, partially mixed estuaries. *Journal of Physical Oceanography*, 34, 2677–2691. Huijts, K.M.H., Schuttelaars, H.M., De Swart, H.E., & Valle-Levinson, A. (2006). Lateral entrapment of sediment in tidal estuaries: An idealized model study. *Journal of Geophysical Research: Oceans*, 111(C12), 1-14. Jung, N.W., Lee, G., Jung, Y., Figueroa, S.M., Lagamayo, K.D., Jo, T.C., & Chang, J. (2021). MorphEst: An Automated Toolbox for Measuring Estuarine Planform Geometry from Remotely Sensed Imagery and Its Application to the South Korean Coast. *Remote Sensing*, 13(2), 330. Kamada, M., Woo, H., & Takemon, Y. (2004). Ecological engineering for restoring river ecosystems in Japan and Korea. *In Ecological Issues in a Changing World,* 337-353. Springer, Dordrecht. https://doi.org/10.1007/978-1-4020-2689-8_21Kang, J.W. (1999). Changes in Tidal Characteristics as a Result of the Construction of Sea-dike/Sea-walls in the Mokpo Coastal Zone in Korea. *Estuarine, Coastal and Shelf Science*, 48, 429-438. https://doi.org/10.1006/ecss.1998.0464Kidd, I.M., Davis, J.A., & Fischer, A. (2017). Total exclusion barrages as sea-level rise mitigators: The geomorphological trade-offs for new installations. *Ocean & Coastal Management*, 143, 122–135. Kim, T.I., Choi, B.H., & Lee, S.W. (2006). Hydrodynamics and sedimentation induced by large-scale coastal developments in the Keum River Estuary, Korea. *Estuarine, Coastal and Shelf Science*, 68(3-4), 515-528. Kwon, H.K., & Lee, S.H. (1999). Physical environment changes in the Keum River Estuary by the dyke gate operation: I. Mean sea level and tide. *Journal of the Korean Society of Oceanography*, 4, 93-100 (in Korean, with English Abstr.).Lee, K.H., Rho, B.H., Choi, H.J.,

& Lee, C.H. (2011). Estuary classification based on the characteristics of geomorphological features, natural habitat distributions and land uses. *The Sea*, 16(2), 53-69. https://doi.org/10.7850/jkso.2011.16.2.053Lee, J.Y., & Lee, J.L. (2007). An analytical study on heavy siltation in the Keum River Estuary after the construction of a dyke. *Journal of Coastal Research*, pp. 1147-1151.Mellor, G.L. (1996). Introduction to Physical Oceanography.Milliman, J.D., & Farnsworth, K.L. (2013). River Discharge to the Coastal Ocean: A Global Synthesis. Cambridge University Press.Morris, R.K.A. (2013). Geomorphological analogues for large estuarine engineering projects: A case study of barrages, causeways and tidal energy projects. *Ocean & Coastal Management*, 79, 52–61. Moskalski, S., Floch, F., & Verney, R., (2020). Suspended sediment fluxes in a shallow macrotidal estuary. *Marine Geology*, 419, 106050. https://doi.org/10.1016/j.margeo.2019.106050Murray-Darling Basin Authority. Water management factsheet [online]. Available at: www.mdba.gov.au/. (Accessed 14 May 2021). Prandle, D. (2009). Estuaries: dynamics, mixing, sedimentation and morphology. Cambridge University Press.Prandle, D., & Rahman, M. (1980). Tidal response in estuaries. *Journal of Physical Oceanography*, 10(10), 1552-1573. Ryu, C.R., & Chang, S.D. (1979). Tide and tidal current in the estuary of the Nakdong River. *Journal of the Oceanographical Society of Korea*, 14(2), 71-77 (in Korean, English abstract).Scully, M.E., & Friedrichs, C.T., (2007). Sediment pumping by tidal asymmetry in a partially mixed estuary. *Journal of Geophysical Research*, 112, C07028. https://doi:10.1029/2006JC003784Sherwood, C.R., Aretxabaleta, A.L., Harris, C.K., Rinehimer, J.P., Verney, R., & Ferré, B. (2018). Cohesive and mixed sediment in the regional ocean modeling system (ROMS v3. 6) implemented in the Coupled Ocean–Atmosphere–Wave–Sediment Transport Modeling System (COAWST r1234). *Geoscientific Model Development*, 11(5), 1849-1871. https://doi.org/10.5194/gmd-11-1849-2018Shin, H.J., Lee, G., Kang, K., & Park, K. (2019). Shift of estuarine type in altered estuaries. *Anthropocene Coasts*, 2(1), 145-170. Sommerield, C.K., & Wong, K.-C., (2011). Mechanisms of sediment flux and turbidity maintenance in the Delaware Estuary. *Journal of Geophysical Research*, 116, c01005. https://doi.org/10.1029/2010JC006462Soulsby, R. (1997). Dynamics of Marine Sands: A Manual for Practical Applications. Thomas Telford.Takahasi, Y. (1997). Water resource development and the environment in Japan. *International Journal of Water Resources Development*, 13(2), 181-186. https://doi.org/10.1080/07900629749818Tarpley, D.R.N., Harris, C.K., Friedrichs, C.T., & Sherwood, C.R. (2019). Tidal variation in cohesive sediment distribution and sensitivity to flocculation and bed consolidation in an idealized, partially mixed estuary. *Journal of Marine Science and Engineering*, 7, 334. Tönis, I.E., Stam, J.M.T., & Van de Graaf, J. (2002). Morphological changes of the Haringvliet estuary after closure in 1970. *Coastal Engineering*, 44(3), 191-203. Traini, C., Proust, J.N., Menier, D., & Mathew, M.J. (2015). Distinguishing natural evolution and human impact on estuarine morpho-sedimentary development: A case study from the Vilaine Estuary, France. *Estuarine, Coastal and Shelf Science*, 163, 143-155. Tilai, L., Liming,

C., Xiangyu, G., & Lei, D. (2019). Analysis of sediment deposition downstream tidal sluice of estuary. In International Conference on Asian and Pacific Coasts (pp. 649-655). Springer, Singapore. https://doi.org/10.1007/978-981-15-0291-0_89Umlauf, L., & Burchard, H. (2003). A generic length-scale equation for geophysical turbulence models. *Journal of Marine Research*, 61(2), 235-265. Van Proosdij, D., Milligan, T., Bugden, G., & Butler, K. (2009). A tale of two macro tidal estuaries: differential morphodynamic response of the intertidal zone to causeway construction. *Journal of Coastal Research*, 772-776.Wang, Z.B., Van Maren, D.S., Ding, P.X., Yang, S.L., Van Prooijen, B.C., De Vet, P.L.M., Winterwerp, J.C., De Vriend, H.J., Stive, M.J.F., & He, Q. (2015). Human impacts on morphodynamic thresholds in estuarine systems. *Continental Shelf Research, Coastal Seas in a Changing World: Anthropogenic Impact and Environmental Responses*, 111, 174–183. Warner, J.C., Armstrong, B., He, R., & Zambon, J.B. (2010). Development of a coupled ocean–atmosphere–wave–sediment transport (COAWST) modeling system. *Ocean Modelling*, 35(3), 230-244. Warner, J.C., Geyer, W.R., & Lerczak, J.A. (2005). Numerical modeling of an estuary: A comprehensive skill assessment. *Journal of Geophysical Research: Oceans*, 110(C5). Warner, J.C., Sherwood, C.R., Signell, R.P., Harris, C.K., & Arango, H.G. (2008). Development of a three-dimensional, regional, coupled wave, current, and sediment-transport model. *Computers & Geosciences*, 34(10), 1284-1306. Webster, I.T. (2005). An overview of the hydrodynamics of the Coorong and Murray Mouth. *CSIRO: Water for a Healthy Country National Research Flagship*, 1-34. https://doi.org/10.4225/08/5867f41b23b59Whitehouse, R.J.S., Soulsby, R.L., Roberts, W., & Mitchener, H.J. (2000). Dynamics of Estuarine Muds: A Manual for Practical Applications. Thomas Telford.Williams, J.R., Dellapenna, T.M., & Lee, G. (2013). Shifts in depositional environments as a natural response to anthropogenic alterations: Nakdong Estuary, South Korea. *Marine Geology*, 343, 47–61. Williams, J., Dellapenna, T., Lee, G., & Louchouarn, P. (2014). Sedimentary impacts of anthropogenic alterations on the Yeongsan Estuary, South Korea. *Marine Geology*, 357, 256–271. Williams, J., Lee, G., Shin, H.J., & Dellapenna, T. (2015). Mechanism for sediment convergence in the anthropogenically altered microtidal Nakdong Estuary, South Korea. *Marine Geology*, 369, 79-90. Winterwerp, J.C., & Wang, Z.B. (2013). Man-induced regime shifts in small estuaries—I: theory. *Ocean Dynamics*, 63(11-12), 1279-1292. Wolanski, E., & Elliot, M. (2016). Estuarine Ecohydrology: An Introduction. Elsevier.Wu, H., & Zhu, J. (2010). Advection scheme with 3rd high-order spatial interpolation at the middle temporal level and its application to saltwater intrusion in the Changjiang Estuary. *Ocean Modelling*, 33, 33–51. Zhu, Q., Wang, Y.P., Gao, S., Zhang, J., Li, M., Yang, Y., & Gao, J. (2017). Modeling morphological change in anthropogenically controlled estuaries. *Anthropocene*, 17, 70–83. https://doi.org/10.1016/j.ancene.2017.03.001